Microscopic Origin of Electron Accumulation in In_2O_3

K. H. L. Zhang and R. G. Egdell*
Department of Chemistry, University of Oxford, Inorganic Chemistry Laboratory, South Parks Road, Oxford OX1 3QR, United Kingdom

F. Offi
CNISM and Dipartimento di Scienze, Università Roma Tre, via della Vasca Navale 84, I-00146 Roma, Italy

S. Iacobucci
CNR-Istituto Fotonica e Nanotecnologie, c/o Dipartimento di Fisica, Università Roma Tre, via della Vasca Navale 84, I-00146 Roma, Italy

L. Petaccia and S. Gorovikov†
Elettra Sincrotrone Trieste, Strada Statale 14 km 163.5, I-34149 Trieste, Italy

P. D. C. King
SUPA, School of Physics and Astronomy, University of St. Andrews, North Haugh, St. Andrews, Fife KY16 9SS, United Kingdom and Kavli Institute at Cornell for Nanoscale Science, Cornell University, Ithaca, New York 14853, USA
(Received 30 August 2012; published 30 January 2013)

Angle-resolved photoemission spectroscopy reveals the presence of a two-dimensional electron gas at the surface of $In_2O_3(111)$. Quantized subband states arise within a confining potential well associated with surface electron accumulation. Coupled Poisson-Schrödinger calculations suggest that downward band bending for the conduction band must be much bigger than band bending in the valence band. Surface oxygen vacancies acting as doubly ionized shallow donors are shown to provide the free electrons within this accumulation layer. Identification of the origin of electron accumulation in transparent conducting oxides has significant implications in the realization of devices based on these compounds.

DOI: 10.1103/PhysRevLett.110.056803 PACS numbers: 73.20.At, 68.47.Fg, 79.60.Dp, 81.15.Hi

Oxide semiconductors such as In_2O_3 and SnO_2 are amenable to degenerate *n*-type doping to give materials which combine optical transparency in the visible region with a high electrical conductivity [1,2]. These so-called transparent conducting oxides (TCOs) are an essential component as the window electrode in liquid crystal displays, light emitting diodes, and solar cells. Sn-doped In_2O_3 (ITO) is the TCO of choice in many applications owing to the high conductivity and high transmittance that may be achieved using routine thin film deposition techniques [2]. In addition, In_2O_3 itself finds application as a gas sensor for detection of oxidizing gases such as ozone, NO_2, and Cl_2 [3].

Despite its undoubted technological importance, many of the basic properties of In_2O_3 have proved to be controversial. In particular, the fundamental band gap has recently been shown to be almost 1 eV smaller than previously assumed [4], leading in turn to the identification of strong downward band bending at the surface of In_2O_3 [5,6]. Thus, the surfaces of In_2O_3 are highly electron rich, as is the case for the other TCO materials [7]. This has important implications for their use in electronic device applications, where a contact must always be made to the surface, as well as for their performance as sensors where molecules are adsorbed on the surface. Recent theoretical work has even suggested that the charge carriers giving unintentional conductivity in nominally undoped In_2O_3 result from surface carriers, rather than from bulk defects or impurities [8]. Surprisingly, however, a microscopic identification of the origin of surface electron accumulation amongst the TCOs has proved elusive.

One major obstacle has been the limited availability of single crystal samples with low unintentional bulk doping. We have recently grown high-quality undoped In_2O_3 and ITO films by oxygen plasma-assisted molecular beam epitaxy [9–11]. Here, angle-resolved photoemission spectroscopy (ARPES) is used to examine the surface electronic properties of such epitaxial $In_2O_3(111)$ and ITO(111) films. A two-dimensional electron gas (2DEG) is observed in the near-surface of In_2O_3, with the host conduction band quantized into subband states by the confining potential well associated with the pronounced downward band bending. It is shown that the density of this surface 2DEG is sufficiently high for many-body interactions to induce a pronounced band gap renormalization close to the surface. Furthermore, we identify the source of these free electrons as doubly ionized surface oxygen vacancies, answering the long-standing mystery of the origin of electron accumulation at TCO surfaces.

Undoped In_2O_3 and 3% Sn-doped In_2O_3 (ITO) films with a thickness of 210 nm and atomically flat surfaces were grown on Y-ZrO_2(111) substrates by oxide MBE [9–11] at a substrate temperature of 700 °C. The initial carrier concentrations for the as-grown In_2O_3 and ITO films were 2×10^{18} cm^{-3} and 4×10^{20} cm^{-3}, respectively, as determined by Hall measurements. The carrier density increased to around 1.5×10^{19} cm^{-3} for the undoped sample after the experimental measurements in ultrahigh vacuum (UHV), a value above the limit for the onset of degeneracy. For the doped sample it was possible to estimate an *in situ* carrier density of 4.5×10^{20} cm^{-3} from measurement of the energy of a plasmon satellite on the In 4*d* shallow core line [12] (see Supplemental Material [13]).

ARPES spectra were measured using photon energies between 6 and 40 eV on the BaDElPh beam line of the Elettra Synchrotron Laboratory, Trieste, Italy [14]. The contribution of second order radiation is estimated to be well below 10^{-4} of the first order contribution at 9 eV photon energy. Measurements were performed at room temperature, in a pressure better than 5×10^{-11} mbar, with a total energy resolution of 100 meV and an angular resolution of 0.25°. The surfaces of In_2O_3 and ITO were cleaned by repeated cycles of Ar^+ sputtering (500 eV) and annealing at 600 °C in UHV for 1 h. The cleanliness of the final surface was confirmed by well-ordered (1×1) low energy electron diffraction (LEED) patterns and the absence of a C 1*s* signal in core level photoemission. Additional experiments were performed offline using He-I radiation ($h\nu = 21.2$ eV).

Figure 1(a) shows photoemission spectra of nominally undoped In_2O_3 and ITO excited at $h\nu = 19$ eV. A well-defined conduction band (CB) feature straddling the Fermi energy is observed for ITO in Fig. 1(b), as expected due to the highly degenerate doping by Sn. Surprisingly, this feature persists in nominally undoped In_2O_3, with a band filling and spectral weight both much larger than would be expected given the 30-fold decrease in bulk carrier density. Furthermore, the valence band onset (VBO) in nominally undoped In_2O_3, is as high as 3.05 eV. This is only slightly less than the value of 3.18 eV for the ITO sample. The shift is significantly smaller than the value of 0.48 eV that would be expected from the bulk doping levels [15].

Overall, these observations are consistent with downward band bending and carrier accumulation in the near surface of the nominally undoped In_2O_3 [5,6,16], such that the Fermi level lies higher relative to the CB minimum at the surface than in the bulk. Here, we use ARPES to demonstrate that the observed CB emission arises from such an increased carrier density at the surface. Angle-resolved spectra were measured at 9 eV photon energy: this corresponds to a maximum in the intensity of the CB feature [see Fig. 1(c) and Supplemental Material [13]] and ensures an effective information depth of around

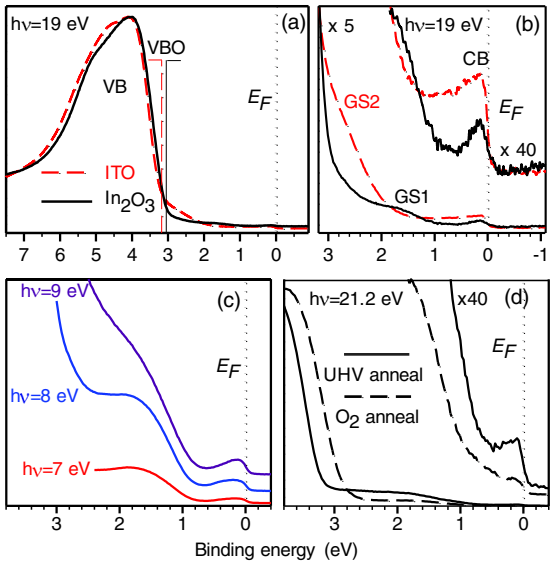

FIG. 1 (color online). (a) Photoemission spectra of In_2O_3(111) and ITO(111) excited at 19 eV photon energy. The positions of the valence band onsets (VBO) derived by linear extrapolation of the band edges are indicated. (b) Expanded view of gap states (GS) and CB states close to the Fermi energy. (c) Spectra of the gap state and accumulation layer electrons for In_2O_3(111) excited at 7–9 eV photon energy. Collection angle is ±7° in (a)–(c). (d) Spectra of nominally undoped In_2O_3(111) excited at $h\nu = 21.2$ eV. Measurements performed after surface preparation by ion bombardment and UHV annealing and then after annealing in oxygen (1×10^{-6} mbar) for 30 min at 600 °C.

40–50 Å [17], comparable with the thickness of the accumulation layer as discussed below. The conduction band feature shows a second weaker and broader maximum in intensity for photon energies around 24 eV (Supplemental Material [13]) and so can also be observed in offline experiments using He-I radiation with $h\nu = 21.2$ eV [Fig. 2(d)]. However, the information depth will have lower values of 20 Å or less at these higher photon energies, which is not sufficient to sample the whole of the accumulation layer.

The ARPES measurements shown in Fig. 2(a) reveal two nested free-electron-like band dispersions, more clearly visible in the second-derivative image of Fig. 2(b). The shallower band has a Fermi momentum of $k_{F1} = 0.08$ $Å^{-1}$ and occupied bandwidth of ~0.1 eV, while the deeper band has $k_{F2} = 0.14$ $Å^{-1}$ and a bandwidth of ~0.4 eV [Fig. 2(c)]. The bulk Fermi level lies only 0.07 eV above the CB minimum. Thus the lower subband cannot be associated with bulk CB states of In_2O_3 as proposed in a recent ARPES study on In_2O_3 bulk crystals [18]. Instead, the ARPES results indicate the presence of a 2DEG localized at the surface. Downward band bending creates a confining potential well perpendicular to the surface. If the well is sufficiently deep and narrow, electrons within the accumulation layer are quantized into 2D subbands, as observed here and also previously, for the intrinsic electron

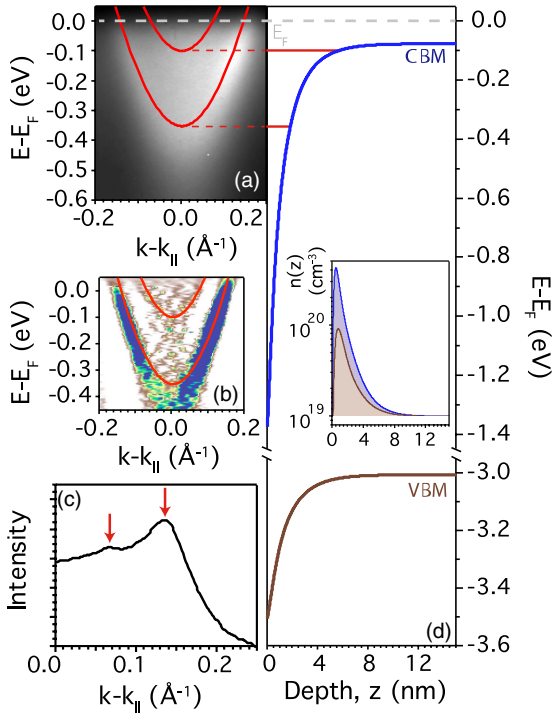

FIG. 2 (color online). (a) ARPES photocurrent map of conduction band states of $In_2O_3(111)$ excited with 9 eV photons, showing two subbands below the Fermi level. The horizontal axis is the momentum ($k_{\|}$) parallel to the surface along $[1\bar{1}0]$, while the vertical axis is the binding energy. The solid curves indicate the positions of two subbands derived from Poisson-Schrödinger calculations. (b) A second-derivative image of the data shown in (a). (c) Momentum distribution curve obtained by summing intensities over a range ± 25 meV with respect to the Fermi level. The points where the subbands cross the Fermi level are indicated. (d) Downward band bending of 1.30 eV in the CB (upper curve) and 0.45 eV in the VB (lower curve) and corresponding quantized 2D states. The inset shows the near-surface carrier density obtained from Poisson-MTFA calculations. The upper and lower curves correspond to band bending of the CB by 1.30 and 0.45 eV, respectively, yielding surface carrier densities of 5.05×10^{13} cm^{-2} and 1.41×10^{13} cm^{-2}.

accumulation layers of InAs [19], InN [20], and CdO [19,21]. The surface charge density n_{2D} giving rise to this 2DEG can be estimated quantitatively from the measured Fermi momenta through the relationship $n_{2D} = \Sigma k_{Fi}^2/2\pi$, giving a total electron density of $n_{2D} = 4.2 \times 10^{13}$ cm^{-2}. This very high density is much larger than typically observed in conventional semiconductor interfaces such as Si metal-oxide-semiconductor field-effect transistors or at the GaAs/AlGaAs interface [22].

To analyze the 2DEG quantitatively, we have carried out nonparabolic coupled Poisson-Schrödinger calculations [23]. The band bending potential was calculated by solving Poisson's equation within a modified Thomas-Fermi approximation (MTFA), allowing for nonparabolicity of the CB through the $\mathbf{k} \cdot \mathbf{p}$ approximation. The one-dimensional Schrödinger equation was then solved to yield the 2DEG density and position of the quantized subbands. Using a bulk free electron density of 1.5×10^{19} cm^{-3}, a downward bending of the conduction band by 1.3 eV was required to obtain agreement with the ARPES data. The calculations then well reproduce the dispersions of the two measured subbands with band minima located at 0.08 and 0.38 eV below E_F. The upper subband is very diffuse and not well defined experimentally at 9 eV photon energy. This band sits very close to the top of the near-surface quantum well, as seen in Fig. 2(d). Consequently, this state cannot be considered a well defined two-dimensional state (as for the lower subband), but will likely retain substantial three dimensional character (i.e., dispersion along $k_{\perp}$) as the confinement energies are so small. ARPES measurements always integrate over a finite window in $k_{\perp}$. This leads to the broad spectral features observed here, and seen previously for the shallow subbands of InAs and CdO 2DEGs [19]. Emission from the upper subband is much stronger than from the deeper subband under 31 eV excitation (Supplemental Material [13]). The effective mass at the bottom of the deeper subband required to fit the band dispersion is $0.22m_e$. This is lower than the value of $0.35m_e$ cited for the conduction electron effective mass of ITO films [24]. However, the conduction band in In_2O_3 is nonparabolic so that the effective mass increases in moving upward from the bottom of the conduction band in highly doped ITO. The effective mass found here is in excellent agreement with that obtained using hybrid density functional theory [25].

Overall, therefore, our Poisson-Schrödinger calculations confirm that quantized states arise within the surface electron accumulation layer produced by downward band bending. It is of interest to note, however, that the downward bending of the CB (1.3 eV) is much higher than the value we extract experimentally for the valence band (VB) bending. Indeed, from the onset of VB photoemission as well as the binding energy of the In 4*d* core level peak [6], we could determine a downward bending of the VB of only 0.45 eV (Supplemental Material [13]), as shown in Fig. 2(d). If this band bending is used for *both* valence and conduction bands, the calculations yield only a single occupied subband and a corresponding carrier density of 1.4×10^{13} cm^{-2} [area beneath bottom curve in inset to Fig. 2(d)], which is significantly lower than the value of 4.2×10^{13} cm^{-2} estimated from ARPES. We propose that the differences in valence and conduction band bending result from many-body interactions caused by the high electron density within the electron accumulation layer, which leads to a pronounced shrinkage of the band gap at the surface of In_2O_3, as for other high-density surface 2DEGs [19]. The shrinkage arises from screening of the interaction between valence and conduction band states by the conduction electrons themselves. The surface band gap shrinkage effectively increases the depth of the potential

well at the surface, giving quantized states at higher binding energies than would be expected from the valence band bending and neglect of these many-body interactions. The band gap renormalization found here is much bigger than in the bulk for comparable carrier densities [15], which may indicate an important role of dimensionality in determining the magnitude of the effect.

Thus, the implications of electron accumulation for device applications are even more striking than might initially be thought, with not just the presence of a near-surface layer that is highly electron rich, but one that even has an electronic structure fundamentally altered from that of the bulk. Yet, the microscopic origins of this electron accumulation have proved elusive. The striking tendency towards electron accumulation across the TCOs has been explained within the charge neutrality level (CNL) concept. In_2O_3, as for the other TCOs, has a highly dispersive lower CB, but a relatively flat topmost VB [4,25,26]. This leads to a CNL that lies well above the conduction band minimum (CBM) of this material, in fact about 0.4 eV above the CBM [5,6]. This high value typically leads to favorable energetics for the formation of donor-type surface states, which are required to induce electron accumulation [5,7,27]. While this simple model seems to have a powerful predictive power, it describes tendencies, and does not *a priori* guarantee the microscopic existence of such surface states. Identification of their microscopic origin is of central importance for gaining control over the surface electronic properties of TCOs, an essential requirement for their incorporation as the active elements in a new generation of transparent oxide electronics requiring rectifying contacts, as well as for improving their use as transparent contacts and sensor materials.

We use photoemission to directly address this question. Figure 1(b) shows expanded photoemission spectra excited at 19 eV encompassing the top of the valence band, the conduction band and the band gap region. In addition to the conduction band feature, a low-lying in-gap state (GS1) is observed at a binding energy of around 1.6 eV for nominally undoped In_2O_3. The gap state is particularly pronounced at lower photon energies around 8 eV as in Fig. 1(c): the information depth is expected to be around 40–50 Å at these low energies [17]. We assign GS1 to a defect level corresponding to doubly occupied oxygen vacancy (V_o) states in the subsurface region of In_2O_3 broadly consistent with its energetic position in recent first-principles calculations [8]. This is further supported by measurements performed after annealing the sample in oxygen, which would be expected to heal oxygen vacancies. As shown in Fig. 1(d), the intensity of the in-gap peak is indeed strongly suppressed following oxygen treatment.

At the same time, we find a drastic shift of the leading edge of the valence band by 0.3 eV toward E_F, and a pronounced suppression of the near-E_F intensity that we have shown above directly reflects the presence of an electron accumulation layer. Together, these observations indicate a reduction of band bending and depopulation of surface electron accumulation as oxygen vacancies are healed in In_2O_3. This reveals that the microscopic origin of the positive surface states which mediate electron accumulation in In_2O_3, and most likely other TCOs, are oxygen vacancies localized at the surface. This is consistent with recent work on the complex oxides $SrTiO_3$ and $KTaO_3$ [28,29] where surface 2DEGs were also found to be accompanied by in-gap oxygen-vacancy-derived states whose spectral weight directly scaled with the density of the 2DEG. Thus, it seems that electron accumulation induced by oxygen vacancies may be a general property of oxide surfaces.

The energy of O-vacancy states and their influence on the (bulk) conductivity of wide band gap semiconductors such as In_2O_3, SnO_2, and ZnO has provoked widespread controversy in the past few years [7,30–32]. Recent work has suggested that although oxygen vacancies are the most stable and abundant defect in the bulk of In_2O_3, the V_o level is too deep to be ionized to generate free electrons at room temperature [8]. However, both the defect formation energy [8,33] and the defect ionization energy [8] are dramatically reduced for surface O ions such that surface O vacancies act as shallow donors, as observed here.

It has been shown by LEED that $In_2O_3(111)$ has a bulk-terminated surface with minor relaxations [34]. In detail, the surface structure involves an alternating sequence of atomic layers with stoichiometry and charge $\{[O^{2-}]_{12}^{24-}[In^{3+}]_{16}^{48+}[O^{2-}]_{12}^{24-}\}$, etc. The energy required to create O vacancies within the topmost O_{12} layer is lowest for the three so-called O1 ions [33]. These ions sit highest at the surface and the energy required to remove one of them is only 0.95 eV, less than half the value for bulk In_2O_3. Assuming surface oxygen vacancies act as two electron donors, the sheet density of the 2DEG implies that only 1.6% of O sites in the outermost O_{12} layer are vacant, a plausible value that would be difficult to detect by core photoemission. The surface O vacancy concentration is something that can be controlled experimentally, enabling taming of the extreme surface electronic properties of TCOs, as we have demonstrated here using oxygen exposure. Moreover, these findings could explain the operation of In_2O_3 as a gas sensor. For example, the selective sensing of NO_2 by In_2O_3 nanowire devices [3] likely results from healing of the surface oxygen vacancies and concomitant reduction of surface conductivity. Engineering the surface atomic coordination of TCOs may therefore give new routes to optimizing signal strengths in gas sensor applications.

The GS1 state is suppressed in Sn-doped $In_2O_3(111)$ and a much stronger state just above the top of the valence band is observed, labeled GS2 in Fig. 1(b). A similar deep structure is observed in photoemission spectra of reduced surfaces of SnO_2 itself [35,36] and, as there, the gap state is

assigned to "lone pair" states localized on surface Sn(II) cations. These arise from an antibonding state of mixed Sn $5s/O\ 2p$ character which further hybridizes with Sn 5p states in noncentrosymmetric surface sites [35,37].

In summary, we have used ARPES to directly image a quantized two-dimensional electron gas at the surface of $In_2O_3(111)$ with an electron density sufficiently high that many-body interactions drive a shrinkage of the band gap close to the surface. The microscopic origin of these electrons is shown to be oxygen vacancies localized at the surface, which have a much reduced formation energy as compared with bulk vacancies and act as doubly ionized shallow donors. This identification suggests the potential to control the surface electronic properties of transparent conducting oxides for applications in electronics and sensors.

We thank D. Lonza for technical assistance during the measurements at Elettra. The Oxford MBE project was funded under EPSRC Grant No. GR/S94148. K. H. L. Z. is grateful to the University of Oxford for support.

*Corresponding author.
russell.egdell@chem.ox.ac.uk
†Present address: Canadian Light Source, Inc., University of Saskatchewan, Saskatoon, Canada.

[1] D. S. Ginley and C. Bright, MRS Bull. **25**, 15 (2000).
[2] C. G. Granqvist and A. Hultaker, Thin Solid Films **411**, 1 (2002).
[3] D. H. Zhang, Z. Q. Liu, C. Li, T. Tang, X. L. Liu, S. Han, B. Lei and C. W. Zhou, Nano Lett. **4**, 1919 (2004).
[4] A. Walsh *et al.*, Phys. Rev. Lett. **100**, 167402 (2008).
[5] P. D. C. King, T. D. Veal, D. J. Payne, A. Bourlange, R. G. Egdell, and C. F. McConville, Phys. Rev. Lett. **101**, 116808 (2008).
[6] P. D. C. King, T. D. Veal, F. Fuchs, C. Y. Wang, D. J. Payne, A. Bourlange, H. Zhang, G. R. Bell, V. Cimalla, O. Ambacher, R. G. Egdell, F. Bechstedt and C. F. McConville, Phys. Rev. B **79**, 205211 (2009).
[7] P. D. C. King and T. D. Veal, J. Phys. Condens. Matter **23**, 334214 (2011).
[8] S. Lany, A. Zakutayev, T. O. Mason, J. F. Wager, K. R. Poeppelmeier, J. D. Perkins, J. J. Berry, D. S. Ginley and A. Zunger, Phys. Rev. Lett. **108**, 016802 (2012).
[9] A. Bourlange, D. J. Payne, R. G. Egdell, J. S. Foord, P. P. Edwards, M. O. Jones, A. Schertel, P. J. Dobson and J. L. Hutchison, Appl. Phys. Lett. **92**, 092117 (2008).
[10] K. H. L. Zhang, V. K. Lazarov, T. D. Veal, F. E. Oropeza, C. F. McConville, R. G. Egdell and A. Walsh, J. Phys. Condens. Matter **23**, 334211 (2011).
[11] K. H. L. Zhang, A. Walsh, C. R. A. Catlow, V. K. Lazarov and R. G. Egdell, Nano Lett. **10**, 3740 (2010).
[12] A. Bourlange, D. J. Payne, R. G. Palgrave, H. Zhang, J. S. Foord, R. G. Egdell, R. M. J. Jacobs, T. D. Veal, P. D. C. King and C. F. McConville, J. Appl. Phys. **106**, 013703 (2009).
[13] See Supplemental Material at http://link.aps.org/supplemental/10.1103/PhysRevLett.110.056803 for discussion of the onset of degeneracy in doped In_2O_3 and conduction band widths; shallow core level photoemission and band bending; variation in the intensity of conduction band features with photon energy; and conduction band electron effective mass.
[14] L. Petaccia, P. Vilmercati, S. Gorovikov, M. Barnaba, A. Bianco, D. Cocco, C. Masciovecchio, and A. Goldoni, Nucl. Instrum. Methods Phys. Res., Sect. A **606**, 780 (2009).
[15] A. Walsh, J. L. F. Da Silva and S. H. Wei, Phys. Rev. B **78**, 075211 (2008).
[16] K. H. L. Zhang *et al.*, Chem. Mater. **21**, 4353 (2009).
[17] F. Offi, S. Iacobucci, P. Vilmercati, A. Rizzo, A. Goldoni, M. Sacchi, and G. Panaccione, Phys. Rev. B **77**, 201101 (2008).
[18] V. Scherer, C. Janowitz, A. Krapf, H. Dwelk, D. Braun, and R. Manzke, Appl. Phys. Lett. **100**, 212108 (2012).
[19] P. D. C. King, T. D. Veal, C. F. McConville, J. Zuniga-Perez, V. Munoz-Sanjose, M. Hopkinson, E. D. L. Rienks, M. F. Jensen, and P. Hofmann, Phys. Rev. Lett. **104**, 256803 (2010).
[20] L. Colakerol *et al.*, Phys. Rev. Lett. **97**, 237601 (2006).
[21] L. F. J. Piper *et al.*, Phys. Rev. B **78**, 165127 (2008).
[22] T. Ando, A. B. Fowler, and F. Stern, Rev. Mod. Phys. **54**, 437 (1982).
[23] P. D. C. King, T. D. Veal, and C. F. McConville, Phys. Rev. B **77**, 125305 (2008).
[24] Y. Ohhata, F. Shinoki, and S. Yoshida, Thin Solid Films **59**, 255 (1979).
[25] F. Fuchs and F. Bechstedt, Phys. Rev. B **77**, 155107 (2008).
[26] P. Erhart, A. Klein, R. G. Egdell, and K. Albe, Phys. Rev. B **75**, 153205 (2007).
[27] P. D. C. King, T. D. Veal, P. H. Jefferson, J. Zúñiga-Pérez, V. Muñoz-Sanjosé, and C. F. McConville, Phys. Rev. B **79**, 035203 (2009).
[28] W. Meevasana, P. D. C. King, R. H. He, S. K. Mo, M. Hashimoto, A. Tamai, P. Songsiriritthigul, F. Baumberger and Z. X. Shen, Nat. Mater. **10**, 114 (2011).
[29] P. D. C. King *et al.*, Phys. Rev. Lett. **108**, 117602 (2012).
[30] J. H. W. Dewit, J. Solid State Chem. **20**, 143 (1977).
[31] S. Lany and A. Zunger, Phys. Rev. Lett. **98**, 045501 (2007).
[32] P. Agoston, K. Albe, R. M. Nieminen, and M. J. Puska, Phys. Rev. Lett. **106**, 245501 (2011).
[33] A. Walsh, Appl. Phys. Lett. **98**, 261910 (2011).
[34] K. Pussi, A. Matilainen, V. R. Dhanak, A. Walsh, R. G. Egdell and K. H. L. Zhang, Surf. Sci. **606**, 1 (2012).
[35] P. A. Cox, R. G. Egdell, C. Harding, A. F. Orchard, W. R. Patterson, and P. J. Tavener, Solid State Commun. **44**, 837 (1982).
[36] J. M. Themlin, R. Sporken, J. Darville, R. Caudano, J. M. Gilles and R. L. Johnson, Phys. Rev. B **42**, 11914 (1990).
[37] A. Walsh, D. J. Payne, R. G. Egdell, and G. W. Watson, Chem. Soc. Rev. **40**, 4455 (2011).